

# A Computational Model of Vortex Ring Formation in Hydrogels

BEE/MAE 4530  
Computer Aided Engineering:  
Applications to Biomedical Processes

Shoshana Das  
Alyssa Fiore  
Dillon Hickman  
Varsha Vasthare

# Table of Contents

<b>1. Executive Summary</b> .....	2
<b>2. Introduction</b> .....	3
A. Theory .....	3
B. Experimental Background .....	3
<b>3. Problem Statement and Design Objectives</b> .....	5
A. Problem Statement: .....	6
B. Design Objectives:.....	6
<b>4. Problem Formulation:</b> .....	6
<b>5. Methods</b> .....	7
<b>6. Results</b> .....	9
<b>7. Conclusions and Future Directions</b> .....	14
<b>8. Appendix</b> .....	15
Appendix A: Mathematical Statement .....	15
Appendix B: Solution Strategy .....	18
Appendix D: References .....	22

# 1. Executive Summary

Duo An, a PhD student at Cornell University, is developing a method that uses electrospray technique to expel clay hydrogel droplets into an ion solution. Upon contact, the droplets crosslink and form various solid geometries, including spheres and toroids. Depending on a few factors, including composition of the hydrogel, volume, viscosity, and speed of falling, the hydrogel will form a variety shapes. Toroidal shapes have many applications because they have a greater surface area to volume ratio than spheres. Therefore, clay hydrogels in the shape of a torus have a greater diffusive capacity than spherically shaped hydrogel formations. This allows for greater mass transfer and thus more efficient drug treatment therapies. The current problem is that the specific conditions that cause micro-toroid formation are not well understood. The majority of An's data has used a larger scale droplet size diameter.

This project aimed to elucidate the formation of a toroid shape by creating a COMSOL® simulation that can model the fluid flow and physics on a smaller scale. A pseudo three-phase model was designed to represent the three parts: the droplet of hydrogel, the air, and the ion solution. However, the model had to be implemented as a two-phase problem, due to the three-phase restraints in COMSOL. This was accomplished by implementing the solution and hydrogel as a single phase by defining an initial ion concentration for both the hydrogel and water bath. Additionally, the particle-tracing feature was used in COMSOL to help track the hydrogel species during the simulation.

A larger scale model with a diameter of 3.0 mm was first developed to demonstrate toroid formation on a larger scale. Performing a sensitivity analysis on particle number, density, diameter and initial velocity showed that initial velocity had the largest impact on formation of the final product. This reflects An's findings that varying initial velocities of the hydrogel droplet leads to different spreading and shape formation. In order to further evaluate the model, simulations with different initial velocities were run and their shape formations were qualitatively compared to images and descriptions from An's data. Success in obtaining vortex formation at the large scale indicated that a smaller scale model could be useful in predicting and understanding micro-toroid formation of these hydrogels.

Next, the model was scaled down to a 500  $\mu\text{m}$  diameter droplet and the results were compared to the larger droplet. When compared, the small model had similar vorticity trends to the large model at a faster rate. In order to compare the model's results to An's, the Reynolds and Weber numbers were calculated and final shape formation images were compared with experimental images for models that matched these numbers. Two of the models showed a similar mushroom shape formation to experimental data.

The use of COMSOL to create a scaled down model of An's work helps to provide a better understanding of the underlying physics behind toroid formation of these clay hydrogels. This understanding will lead to better control of the process, in order to produce hydrogels of desired geometries and dimensions, which could give promise for production in future biomedical applications.

## **2. Introduction**

### **A. Theory**

Hydrogels are an emerging technology in the biomedical field. Hydrogel technology allows for many in-vitro applications including cell encapsulation and protein synthesis. An important factor in the use of hydrogels is their ability to perform mass transfer with their environments. A high rate of mass transfer could be essential in achieving efficient exchange of therapeutic products between hydrogel and treatment site.

Different 3D geometries can have very different surface area to volume ratios. Currently a sphere is the most common shape used in hydrogel technology. The geometry of a toroid has greater surface area per unit volume compared to a sphere. This gives the shapes a higher rate of mass transfer, which has implications for faster drug flux and exchange of cell nutrients and waste. This higher rate of cell nutrient and waste exchange increases cell viability [1]. Therefore, the creation of a method for generating toroid hydrogels could both increase the rate of transfer from hydrogel to outside environment and aid in cell viability.

Past studies have already looked at the use of toroid shapes for drug delivery, investigating these important mass transfer properties of hydrogels and tori. Hydrogels have been used as cell encapsulation devices due to their similar three-dimensional structure and mechanical properties to native tissue scaffolds [2]. Cell encapsulation refers to the technique of trapping cells in three-dimensional tissue scaffold, and cells can then be delivered into other tissues by injection for therapeutic purposes. For instance, pancreatic cells encapsulated in hydrogels can be injected into the liver, causing insulin secretion without autoimmune response [3]. This functionality is manifested due to the structure of scaffolds, which have matrix sizes that can theoretically be small enough to prevent encapsulated cells from escaping and foreign objects from entering, yet large enough to allow for nutrient and waste exchange and the controlled diffusion of a therapeutic drug. The application of tori to cell encapsulation has promising results.

Clay hydrogels have also been demonstrated to catalyze the polymerization of RNA and are used in cell-free protein production for therapeutic purposes [4]. The enhanced mass transfer conferred by hydrogels leads to increased flow of transcriptional and translational reagents into the gels, as well as increased export of protein products. Given that a donut-shaped torus theoretically has greater surface area than a sphere of the same volume at certain dimensions, a torus should have greater mass transfer capabilities. This has interesting implications in choosing the geometry of a cell-encapsulating scaffold.

### **B. Experimental Background**

Duo An, a Ph.D. student working at Cornell University, has identified the necessity of investigating the torus morphology because of its relevance to medical treatments. Specifically, he is investigating the relevance of high mass transfer capabilities that this geometry has to the islet treatment of Type I Diabetes, which relies on mass transfer through the capsules. He is using hydrogel because of its practical applications in treatment therapies. An's experimental set up is shown in Figure 1.

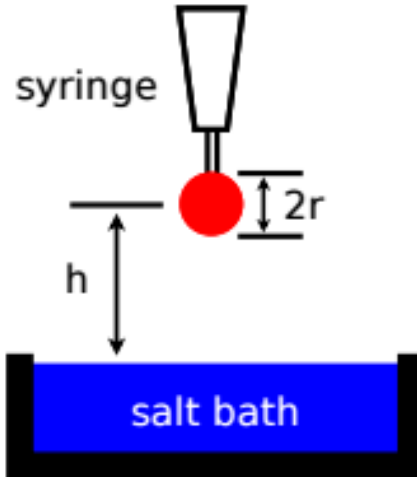


**Figure 1.** Illustration of experimental set up by Duo An. A hydrogel droplet (red) is released at a known height into a crosslinking ion bath (blue).

A hydrogel droplet is released via electro spray technique from a measured height into a crosslinking water bath. The droplet falls into a  $\text{Ca}^{2+}$  solution and crosslinks with the ions in the solution to form a solidified shape over time. Images were taken using a high-speed camera to show the formation and crosslinking process the hydrogel undergoes (Figure 2).

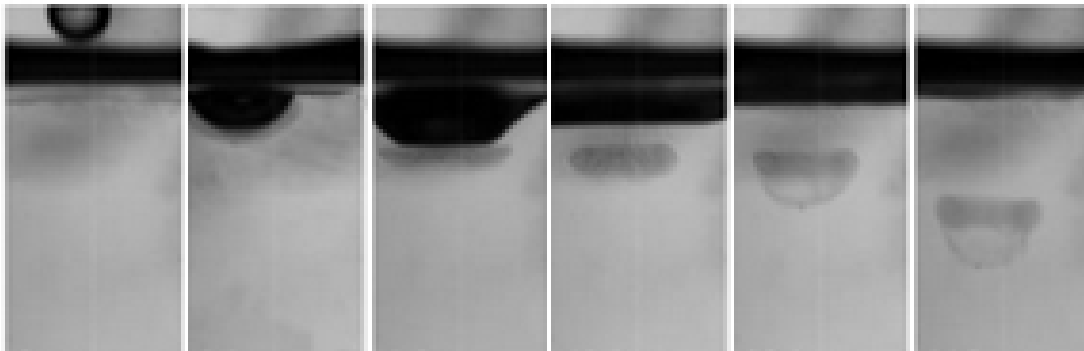


**Figure 2.** Time-lapse series of hydrogel formation into a torus geometry. The series of photos, which moves from the left to the right, depicts the experimental process.

Figure 2 depicts a droplet that vortexes into a torus shape. Images from left to right depict the hydrogel movement from first impact to formation of final shape. Experiments have been performed at a variety of hydrogel droplet sizes (0.50 mm – 3.0 mm), densities, viscosities, and release heights. Variance of these factors results in formation of other solidified shapes including blobs, mushrooms, caps and fractures. Figure 3 summarizes the different resulting hydrogel geometries over a range of Reynolds ( $Re$ ) and Weber ( $We$ ) numbers that were calculated for each experiment (Eq. 1-2).

$$Re = \frac{\rho v r}{\mu} \quad (1)$$

$$We = \frac{\rho v^2 r}{\sigma} \quad (2)$$

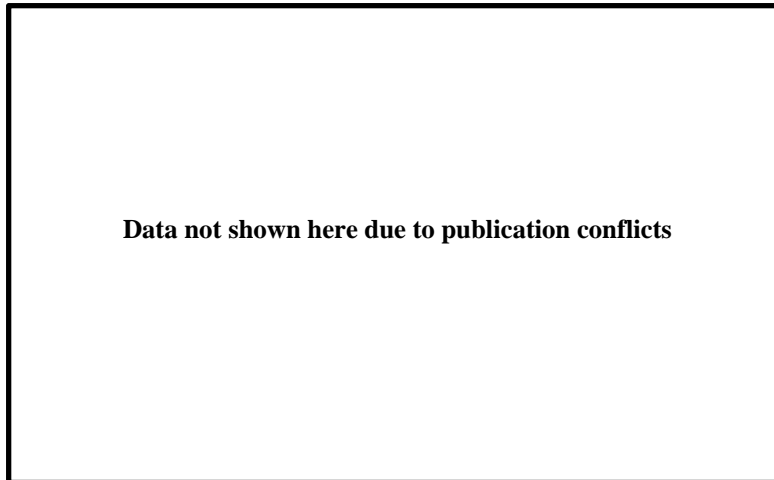


**Figure 3.** Summary of resulting geometries based on calculated Reynolds and Weber numbers of the hydrogel droplet. Observed results include: tori, fractures, mushrooms, blobs and caps.

As can be seen in Figure 3, certain regions of the graph have different geometries based on these two values. At low Re numbers, the resulting shapes are typically blobs and caps, while the desired torus only forms at the higher end of the Re range. As the Weber number increases to its highest values, the model results in fractured hydrogels.

Experimental data to determine Reynolds and Weber numbers are more difficult to obtain for the micro-sized droplets due to the increased speed and small size of experiments. For this reason experimental procedure can more easily investigate shape formation for larger scaled droplets. The experimental research project is novel because the experiments and simulations of the formation of torus-shaped hydrogels by electrospray deposition will add to findings of previous literature [5]. This will aid in the development of more efficient drug diffusion therapies. The research goal aims to elucidate the physics of torus formation by creating a COMSOL simulation of a hydrogel droplet falling into a crosslinking buffer.

### **3. Problem Statement and Design Objectives**

### **A. Problem Statement:**

The goal of this project was to create a COMSOL model that matches experimental findings of shape formation when a hydrogel droplet enters a saline solution.

### **B. Design Objectives:**

1. Determine important factors in geometric formation
2. Create a 3.0 mm diameter model that is comparable to experimental data
3. Create a 500  $\mu\text{m}$  diameter model that can predict experimental behavior on a smaller scale
4. Confirm development of vortexing in COMSOL model
5. Form a toroid shape with the computational model

## **4. Problem Formulation:**

The COMSOL model takes a two-phase flow system approach in order to simulate the three-phase system consisting of air, a droplet of hydrogel, and a saline solution. The problem was formulated by combining the droplet and ion solution in a single phase due to COMSOL's lack of a three-phase solver. The model depicted in Figure 4 uses a 2D axisymmetric geometry in order to model the gel precursor falling through air, into a saline solution.

*Schematic:*

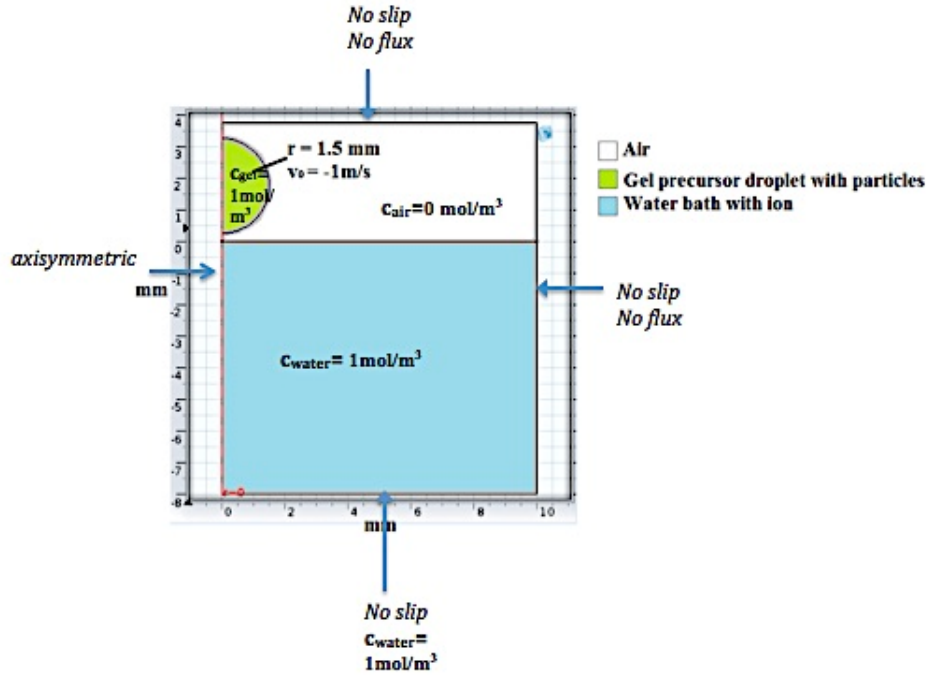


**Figure 4. Schematic.** The schematic above shows the 2D axisymmetric set up of the 1.5mm radius model on COMSOL. Please note that the schematic for the 250-micron radius model, located in the appendix, is six times smaller. The physics of this model encompasses a number of different governing equations in order to correctly define the fluid dynamics of a multi-phase system as well as enable the tracking of the hydrogel in the solution.

## 5. Methods

The COMSOL model is governed by four different physics: the incompressible Navier-Stokes equations, Phase Field equations, Mass Transfer of Diluted Species, and the Sum of Forces equation. Parameters and variables used are defined in Table A1. Coupling the fluid equations with mass transfer allowed for the model to track the droplet of hydrogel as it vortexed in the saline solution. The first physics, governed by the Navier-Stokes (Eq. 3-4), describes the transport behavior and momentum of both the air and water phases in all domains of the geometry. A no slip boundary condition has been implemented for all external boundaries.

$$\text{Navier-Stokes: } \rho \left( \frac{\partial u_r}{\partial t} + u_r \frac{\partial u_r}{\partial r} + u_z \frac{\partial u_r}{\partial z} \right) = -\frac{\partial P}{\partial r} + \rho g_r + \mu \left[ \frac{1}{r} \frac{\partial}{\partial r} \left( r \frac{\partial u_r}{\partial r} \right) - \frac{u_r}{r^2} + \frac{\partial^2 u_r}{\partial z^2} \right] \quad (3)$$

$$\rho \left( \frac{\partial u_z}{\partial t} + u_r \frac{\partial u_z}{\partial r} + u_z \frac{\partial u_z}{\partial z} \right) = -\frac{\partial P}{\partial z} + \rho g_z + \mu \left[ \frac{1}{r} \frac{\partial}{\partial r} \left( r \frac{\partial u_z}{\partial r} \right) + \frac{\partial^2 u_z}{\partial z^2} \right] \quad (4)$$

In addition to Navier Stokes that model fluid mechanics, the Phase Field equation (Eq. 5) was implemented in order to model the fluid dynamics between the surface of the air and water

phases. The equation that governs the interface between the air and aqueous phases tracks the interface as it changes with respect to time. By defining the order parameter  $\phi$ , a function that defines the phase transition can be created between the two different phases, where one phase is defined at the maximum  $\phi$  and the second phase at a minimum  $\phi$ . The phase field smooths the density and viscosity of the fluids in a thin layer at the boundary, giving smooth functions for each of these parameters instead of a step function, which COMSOL would not be able to compute.

$$\text{Phase Field: } \frac{\partial \phi}{\partial t} + \nabla \cdot (\mathbf{u}\phi) = \nabla \cdot \frac{3X\epsilon_{pf}\sigma}{\sqrt{g}} \nabla (-\nabla \cdot \epsilon_{pf}^2 \nabla \phi + (\phi^2 - 1)\phi + \frac{\epsilon_{pf}\sqrt{g}}{3} \frac{\partial f}{\partial \phi}) \quad (5)$$

Coupling the fluid equations with mass transfer of diluted species was necessary in order to track the difference between the hydrogel and ion bath during vortex formation. The droplet, with an initial velocity, falls through the air and into the solution. Upon contact, the diluted species of the hydrogel and solution diffuse into each other allowing visualization of the behavior of the hydrogel material. Defining an arbitrary diluted species concentration in the solution and the hydrogel droplet allows the model to differentiate the hydrogel from the ion bath. The model was unable to encompass the hydrogel crosslinking reactions due to complications with execution in the COMSOL program and the time limitations of the project. The equation had the transient and diffusion terms present. The convection and rate terms are dropped.

$$\text{Mass Transfer of Diluted Species: } \frac{\partial c}{\partial t} = D \left( \frac{1}{r} \frac{\partial}{\partial r} \left( r \frac{\partial c}{\partial r} \right) + \frac{\partial^2 c}{\partial z^2} \right) \quad (6)$$

For mass transfer, no flux boundary conditions were applied at the top and right boundaries. A constant concentration (equal to the initial concentration of ion in bath of 1 mol/m<sup>3</sup>) boundary condition was applied to the bottom boundary. There was no boundary condition necessary for the left boundary, which is an internal boundary for the 2D axisymmetric geometry. Initial conditions of both of the diluted species in the respective domains were 1mol/m<sup>3</sup>. This value was arbitrarily set in order to allow us to visualize the species movements qualitatively. In addition to tracking the difference between the hydrogel and ion bath using two diluted species, the model also tracks the movement of hydrogel particles in the solution over time using particle tracing. The purpose of particle tracing is to visualize the particle shape formation in the saline solution. The sum of forces applied on the particles is described using the below force equation (7). The applied force comes from the coupling of this physics with that of the fluid flow.

$$\text{Sum of Forces: } \frac{\partial(mv)}{\partial t} = F_a + F_d + mg \quad (7)$$

The particle tracing, combined with the diluted species equation aided in visualization and validation of shape formation in the model.

$$v = \sqrt{2gh} \quad (8)$$

Lastly, the initial velocity of the droplet in the model was calculated using a similar range as what was tested experimentally. These velocities were simply calculated from the initial drop height using Eq. 8. These initial conditions, along with the geometry, had to be changed for both the 3.0 mm and 500 μm diameter models.

## 6. Results

The main goals of this project were to create a 3.0 mm diameter COMSOL model with data that is comparable to An’s data on hydrogel toroid shape formation, and to create a 500 μm diameter model that is capable of predicting experimental behavior. The following section details the results obtained from the 3mm and 500μm models in relation to An’s data.

### *Sensitivity Analysis:*

Starting with the 3.0 mm diameter model, particle tracing was used to visualize the formation of the vortex. A sensitivity analysis was performed on the number, size, and density of the particles to reveal their effects on the maximum spreading of hydrogel particles in the solution.

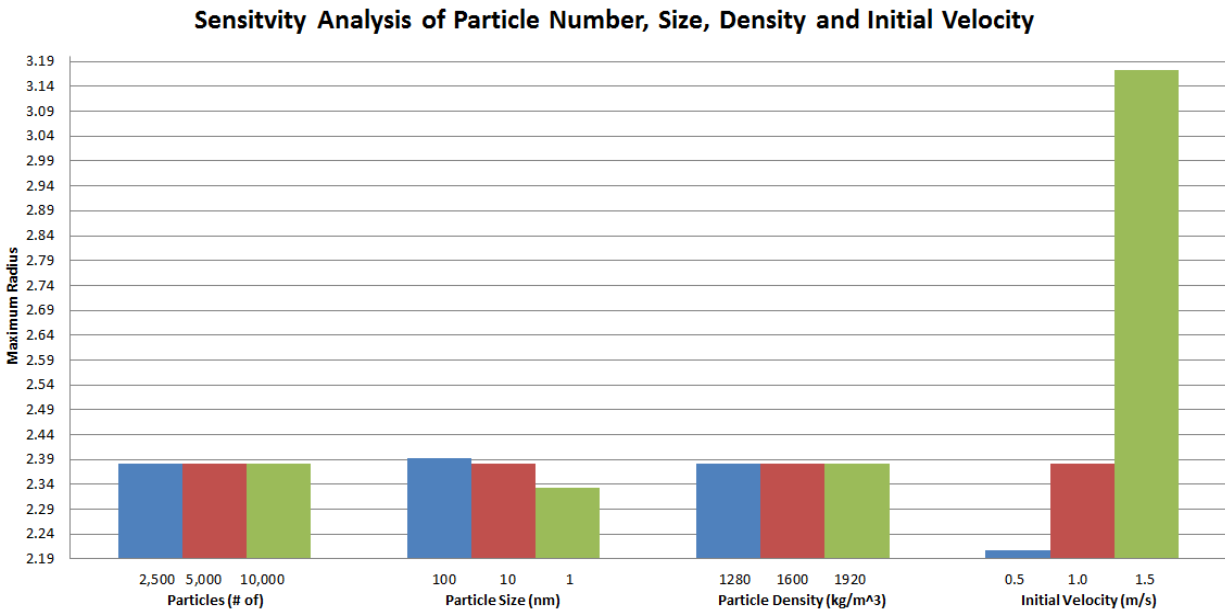


**Figure 5.** Sensitivity Analysis was performed on the number of particles, size of particles, particle density and the initial velocity on model.

The number of particles and the density of the particles did not appear to be significant when varied -50% and +100% for the particle number and +20% and -20% for the particle

density both from a baseline model. It was found that the initial velocity that the droplet of hydrogel was propelled from had the most significant effect. When released at 1.5 m/s (+50%) there was a 33.2% maximum radius increase. There was a less significant decrease of 7.3% when velocity was decreased to 0.5 m/s (-50%). The size of the particles had a lesser effect on the particle spreading; however as the particle size was decreased there was an increasing effect on its impact. Decreasing the particle size by a factor of 10 showed a 2.0% decrease in radius, while increasing by the same factor only had a 0.5% increase.

To confirm the presence of a vortex and visualize the shape formed in the 3.0 mm diameter model, time-lapse images were created of the vorticity, particle location overlaid onto ion concentration, and the 3D isosurface.

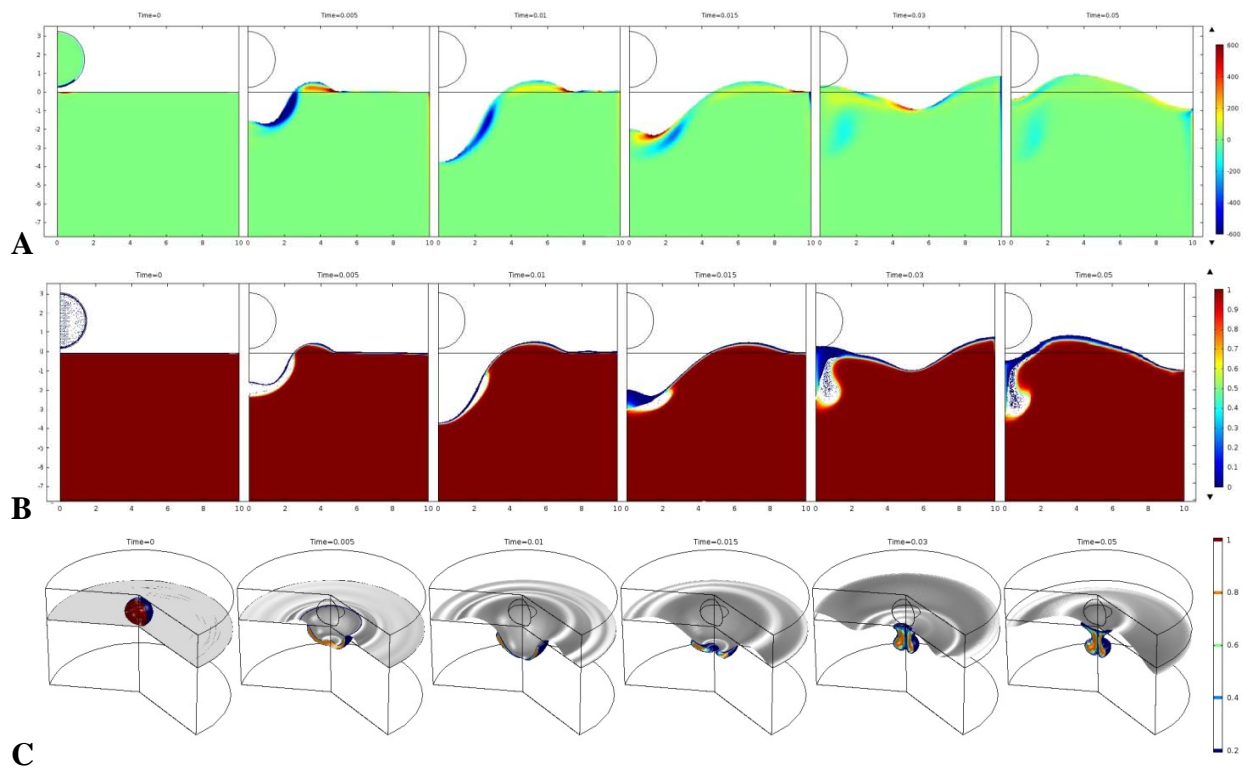


**Figure 6.** Large model with initial droplet velocity -1.0 m/s. From left to right, images are shown at 0, 5, 10, 15, 30, and 50 ms. A: vorticity. B: particle tracing overlaid on concentration of water bath ion. C: isosurfaces showing water surface (gray) and concentration of hydrogel precursor.

Vorticity is the local spinning of the fluid, and the color on Figure 6A shows the magnitude of vorticity, with darker blues or reds indicating stronger local spinning of the fluid. In this graph, blue indicates counterclockwise rotation, and red indicates clockwise rotation. As the fluid surface recoils after the hydrogel precursor droplet has entered the water bath, a vortex forms, which can be seen in the progression of images in Figure 6. The turquoise region that forms on the graph after 15 ms in the region  $0 \leq r \leq 4$  mm and  $-5 \leq z \leq -1$  mm is the vortex.

As time progresses, the region of negative vorticity grows larger and decreases in intensity due to the diffusion of momentum from frictional forces in the fluid.

Particle tracing was used to track the location of the hydrogel precursor, but the forces on the particles were not ideally representative of the entire volume of the hydrogel precursor. As can be seen in Figure 6B, at 30 ms, a region of blue is visible. In this time-lapse sequence, red indicates the presence of the water bath ion and blue shows fluid without a significant concentration of the ion from the water bath. The particles are shown as white dots. The presence of a blue region in this graph without particles shows that the particles did not remain throughout the fluid that was initially in the hydrogel precursor droplet, however the lack of particles in the red regions shows that particles did not diffuse out of the initial droplet fluid.

While Figure 6A and Figure 6B show a plane within the 2D axisymmetric geometry of the model, Figure 6C shows a 3D representation of the model for simpler visualization of results. Similar plots were created for the 500  $\mu\text{m}$  diameter model to validate the small model with similar trends to the larger model.

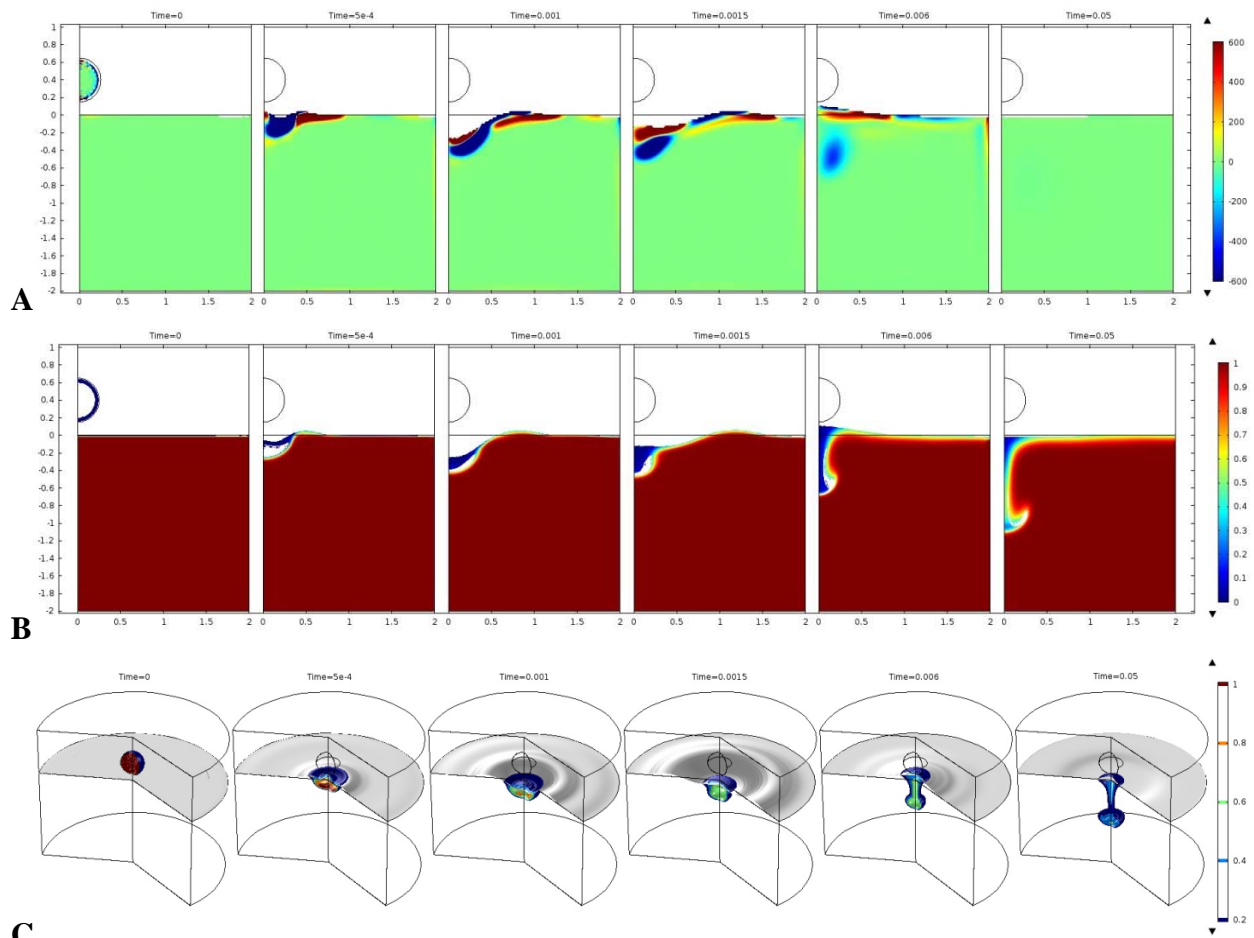


**Figure 7.** Small model with initial droplet velocity -1.25 m/s. From left to right, images are shown at 0, 0.5, 1, 1.5, 6, and 50 ms. A: vorticity. B: particle tracing overlaid on concentration of water bath ion. C: isosurfaces showing water surface (gray) and concentration of hydrogel precursor.

The results from the smaller model were similar to those of the larger model, but occurred approximately ten times faster. In Figure 7A, a turquoise region of counterclockwise vortexing forms in a location similar to the vortex formed in the large model. In Figure 7B, similar to Figure 6B, a region without water bath ion or particles forms, indicating that the forces on the particles were not ideal in either size model. Again, the isosurface time-lapse sequence shows a 3D representation of the overall shape formed by the hydrogel precursor droplet.

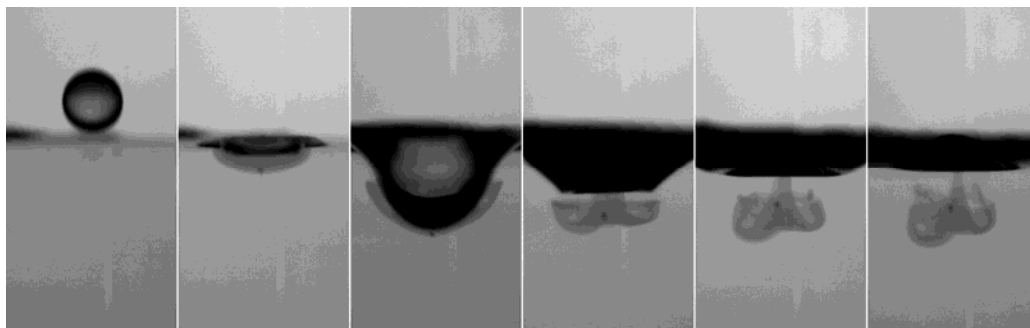


**Figure 8.** Time-lapse sequence showing mushroom formation. The left images shows the initial droplet entering the solution, and the right image shows an upside down mushroom with a cap and stalk.

An example of an experimentally formed mushroom shape can be seen in Figure 8, with a cap-like structure and a stalk similar to the final shape of some of the COMSOL models. Computing the Weber and Reynolds numbers allowed comparison of model results to the experimental results.

**Data not shown here due to publication conflicts**

**Figure 9.** This image shows the plotted experimental data overlaid with calculated model data, indicated by the circles. The black circles highlight calculated model data for the large droplet model, and the red circles highlight calculated model data for the small droplet model.

Figure 9 above shows An's graph of data with our model's results imposed. The larger drop's model overshoots the highest experimental values of Reynolds number. This was due to the use of a two-phase COMSOL model, which restricted the ability to have different viscosities for the hydrogel precursor and ion water bath. The experimental value for the hydrogel precursor from An's experiments was 2.66 cP, however the model used the viscosity of 1.01 cP. This meant that Re number for the droplets was a factor of 2.6 too large. However, when the Re and We for the smaller droplet were calculated, they were found to match ones obtained from experimental data. This enabled for a comparison of the small droplet's hydrogel formations with images from the experimental data. Figure 10 below shows final formation shapes for the large and small models that were run.

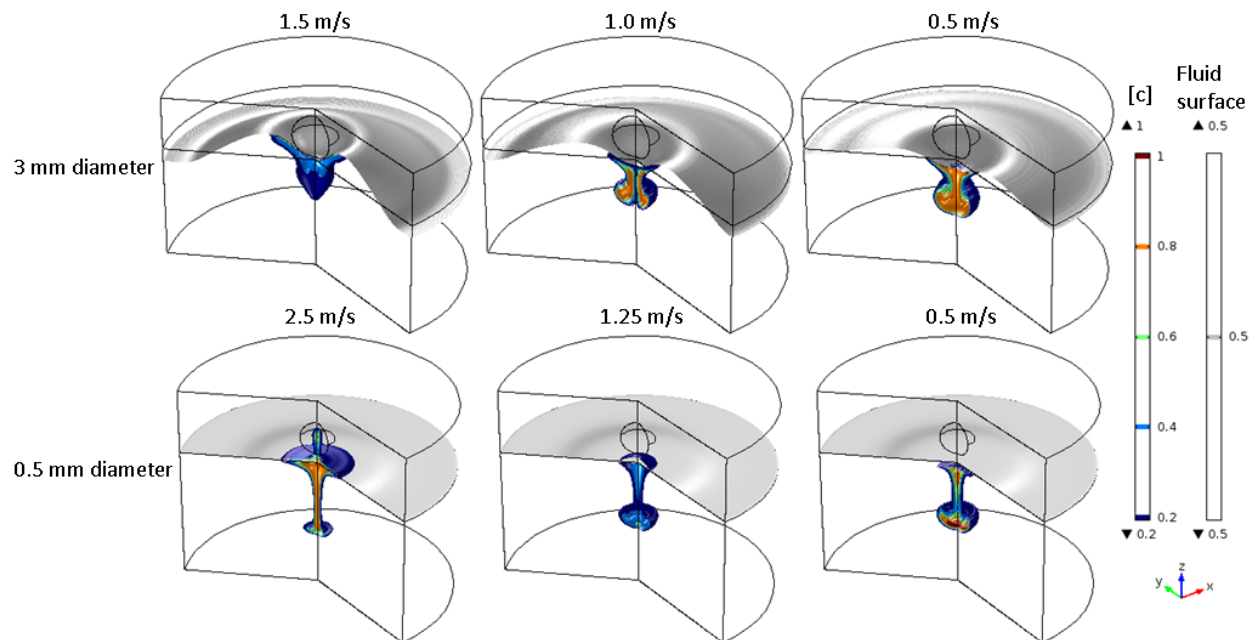


**Figure 10.** Isosurface of final shape formed from each model at 50ms. The 3mm diameter model at 1.0 m/s and 0.5 m/s and the 0.5 mm diameter model at 1.25 m/s and 0.5m/s formed a mushroom shape. The other two models on the left column did not, however.

The 3.0 mm isosurface, shown above, indicates that mushroom shapes are formed at 1.0 m/s and 0.5 m/s and a blob shape at 1.5 m/s. However, as indicated in Figure 9, the 3.0 mm droplet model was unable to be validated because Reynolds and Weber numbers were inconsistent with experimental values.

The 0.5 mm model at 1.25 m/s and 0.5 m/s formed a mushroom shape at 50 ms, similar to the final shape observed in the experimental imaging of the mushroom shape in Figure 8. Additionally, the Reynolds and Weber values in the 0.5 mm model were consistent with experimental data, as observed in Figure 9. The 0.5 mm model at 2.5 m/s did not form the expected toroid shape despite the model having consistent Reynolds and Weber values with the experimental data. Although the model was unable to form the desired shape, it was still successful in tracking shape formation in the simulation.

## **7. Conclusions and Future Directions**

This computational model was successfully able to track the formation of a hydrogel droplet falling into a crosslinking buffer. The model allowed for the visualization of the physics of formation and final geometries with similar Reynolds and Weber numbers were able to be compared to An's experimental results. Additionally, the initial velocity of the droplet was found to have the largest impact of spreading upon contact. A larger 3.0 mm scale model was created that reflected on the experimental conditions and this was successfully scaled down to a 500  $\mu\text{m}$  diameter. This micro-model could be useful in predicting hydrogel behavior in an experimental and production settings. Success in a simple and predictable production method gives implications for this hydrogel production method in faster and more efficient flux drug delivery methods. A better understanding of the method of vortex ring formation will provide researchers with an opportunity to investigate drug release profiles of efficiently-formed tori to investigate mass transfer capabilities.

This model had notable computational design limitations. Areas of investigation for future studies include incorporating a three-phase model to differentiate between the properties such as viscosity of the crosslinking ion bath and the hydrogel precursor. This could be done by defining the viscosity of the aqueous phase as a function of the concentrations of the diluted species within. Additionally the mass transfer equations should include the crosslinking process. This could be implemented as a reaction rate that describes the process of gelation of the hydrogel precursor as it comes into contact with the ion solution. The inclusion of these processes would reduce physical approximation error and hopefully better represent the experimental process.

## **8. Appendix**

### **Appendix A: Mathematical Statement**

The below schematic is of the smaller 0.5 mm model.

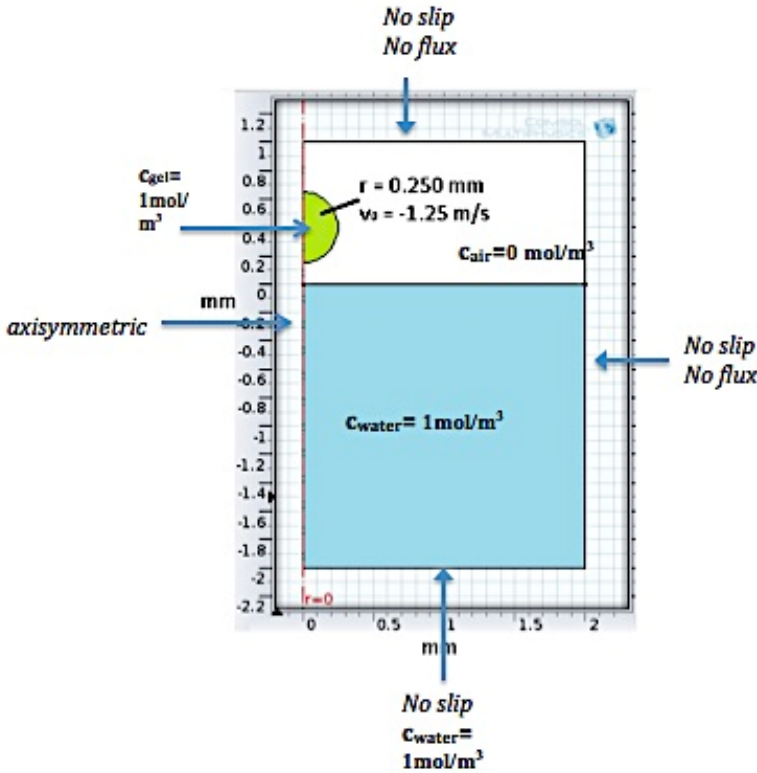


**Figure A1.** 0.5 mm model schematic, including boundary conditions and initial conditions.

The figure above shows the schematic, including initial conditions and boundary conditions for the 0.5 mm model. Note that the schematic is roughly six times smaller than the 1.5 mm model. Below is the list of governing equations used in the computations of the model.

*Navier-Stokes:*

$$\rho \left( \frac{\partial u_r}{\partial t} + u_r \frac{\partial u_r}{\partial r} + u_z \frac{\partial u_r}{\partial z} \right) = -\frac{\partial P}{\partial r} + \rho g_r + \mu \left[ \frac{1}{r} \frac{\partial}{\partial r} \left( r \frac{\partial u_r}{\partial r} \right) - \frac{u_r}{r^2} + \frac{\partial^2 u_r}{\partial z^2} \right] \quad (1)$$

$$\rho \left( \frac{\partial u_z}{\partial t} + u_r \frac{\partial u_z}{\partial r} + u_z \frac{\partial u_z}{\partial z} \right) = -\frac{\partial P}{\partial z} + \rho g_z + \mu \left[ \frac{1}{r} \frac{\partial}{\partial r} \left( r \frac{\partial u_z}{\partial r} \right) + \frac{\partial^2 u_z}{\partial z^2} \right] \quad (2)$$

Initial Condition:  $u$ =initial velocity of droplet

Boundary Conditions:  $u=0$  (no slip) at all external boundaries

*Phase Field:*

$$\frac{\partial \varphi}{\partial t} + \nabla \cdot (\mathbf{u}\varphi) = \nabla \cdot \frac{3X\epsilon_{pf}\sigma}{\sqrt{g}} \nabla (-\nabla \cdot \epsilon_{pf}^2 \nabla \varphi + (\varphi^2 - 1)\varphi + \frac{\epsilon_{pf}\sqrt{g}}{3} \frac{\partial f}{\partial \varphi}) \quad (3)$$

*Mass Transfer of Diluted Species:*

$$\frac{\partial c_A}{\partial t} = D_{AB} \left( \frac{1}{r} \frac{\partial}{\partial r} \left( r \frac{\partial c_A}{\partial r} \right) + \frac{\partial^2 c_A}{\partial z^2} \right) \quad (4)$$

Initial conditions:  $c_{\text{gel}} = 1 \text{ mol/m}^3$ ,  $c_{\text{water}} = 1 \text{ mol/m}^3$ ,  $c_{\text{air}} = 0 \text{ mol/m}^3$

Boundary Conditions:  $\frac{dc_A}{dr} = 0$ ,  $\frac{dc_A}{dz} = 0$  (no flux) at top and left external,  $c_{\text{water}} = 1 \text{ mol/m}^3$  (constant concentration) at the bottom external boundary.

*Sum of Forces:*

$$\frac{\partial(mv)}{\partial t} = F_a + F_d + mg \quad (5)$$

Initial conditions:  $v = \text{Initial velocity of the particles in hydrogel precursor.}$

Below is the list of the parameters that were used for the above governing equations for both the 0.5 mm and 1.5mm model.

**Table A1.** Parameters and variables used to solve governing equations

Physics	Definition	Value	Units	Source
<b>Geometry</b>	Droplet radius	0.25, 1.5	mm	Duo An
<b>Laminar Two-Phase Field</b>	Temperature	293.15	K	COMSOL default
	Air density	1.2044	kg/m <sup>3</sup>	COMSOL default
	Air dynamic viscosity	1.8140e-5	Pa*s	COMSOL default
	Water density	999.62	kg/m <sup>3</sup>	COMSOL default
	Water dynamic viscosity	1.0094e-3	Pa*s	COMSOL default
	Surface tension	0.07246	N/m	COMSOL default
	Parameter controlling interface thickness, $\epsilon_{pf}$	tpf.hmax/2	mm	½ of maximum element size
	Mobility tuning parameter, $X$	8	m*s/kg	Proportional to initial droplet velocity
	Initial droplet velocity	-0.5, -1.25, -2.5; -0.5, -1.0, -1.5	m/s	Duo An
<b>Transport of Diluted Species</b>	Diffusion coefficient of species 1 and species 2	1e-10[m <sup>2</sup> /s]*(8*((tp f.Vf2-.5) <sup>3</sup> )+1e-6)	m <sup>2</sup> /s	Arbitrary
	Species 1 concentration in hydrogel precursor droplet	1	mol/m <sup>3</sup>	Arbitrary
	Species 2 concentration in hydrogel precursor droplet	1	mol/m <sup>3</sup>	Arbitrary
<b>Particle Tracing for Fluid Flow</b>	Particle density	1280, 1600, 1920	kg/m <sup>3</sup>	Arbitrary
	Particle diameter	1e-7, 1e-8, 1e-9	m	Arbitrary
	Release time	0	s	
	Release velocity	-0.5, -1.25, -2.5; -0.5, -1.0, -1.5	m/s	Duo An
	Number of particles per release	2500, 5000, 10000	N/A	Arbitrary

## Appendix B: Solution Strategy

This model was solved using three sequential studies. All studies used a free time step. Study 1 computed the Laminar Two-Phase Flow, Phase Field physics using the PARDISO

solver, had a relative tolerance of 0.01 and a scaled absolute tolerance of  $5.0e-4$ . Study 2 computed the Transport of Diluted Species physics using the PARDISO solver, had a relative and scaled absolute tolerance of  $1e-4$ , and used the fluid velocity field calculated in Study 1. Study 3 computed the Particle Tracing for Fluid Flow physics using the MUMPS solver, had a relative and scaled absolute tolerance of  $1e-4$ , used the fluid velocity field calculated in Study 1, and used the diluted species concentrations calculated in Study 2.

### *Meshes*

Both the 3.0 mm and 500  $\mu\text{m}$  diameter used a free triangular mesh.

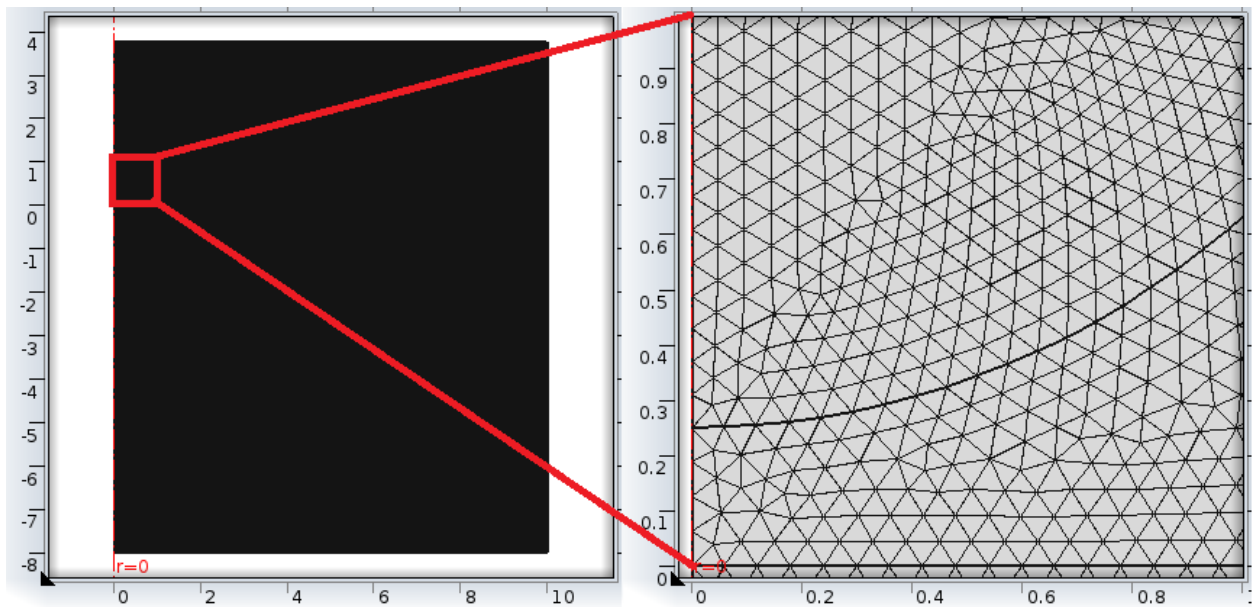


**Figure A1.** Image of entire mesh for 3.0 mm diameter droplet model, with zoomed in image of 1.0 mm x 1.0 mm square.

The large model used a maximum element size of 0.06 mm, resulting in 199466 domain elements and 1458 boundary elements.

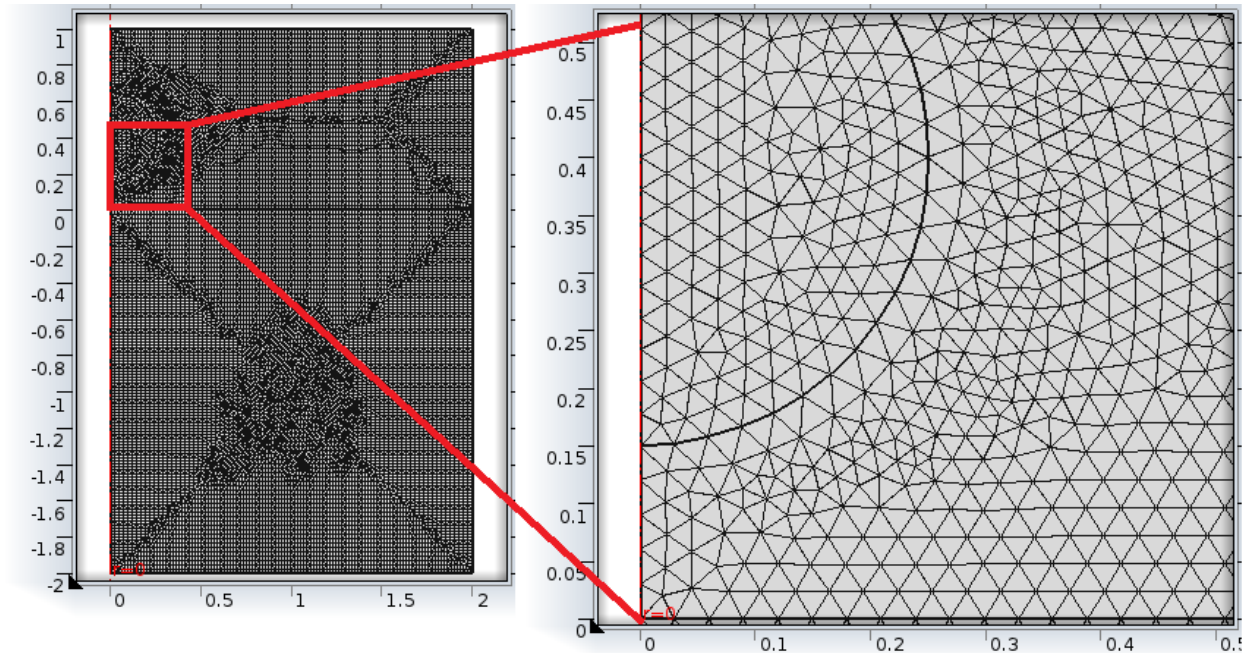


**Figure A2.** Image of entire mesh for 500  $\mu\text{m}$  diameter droplet model, with zoomed in image of 0.5 mm x 0.5 mm square.

The small model used a maximum element size of 0.03 mm, resulting in 151626 domain elements and 1280 boundary elements. For both models a higher density mesh was used at the interfaces with largest changes.

### *Mesh Convergence*

Mesh convergence was performed on total mass of the process over the time range (Figure A3). Due to the nature of the process, COMSOL solved this model as a non-conservative form problem. Meaning that the over the process very small amounts of mass fluctuated.

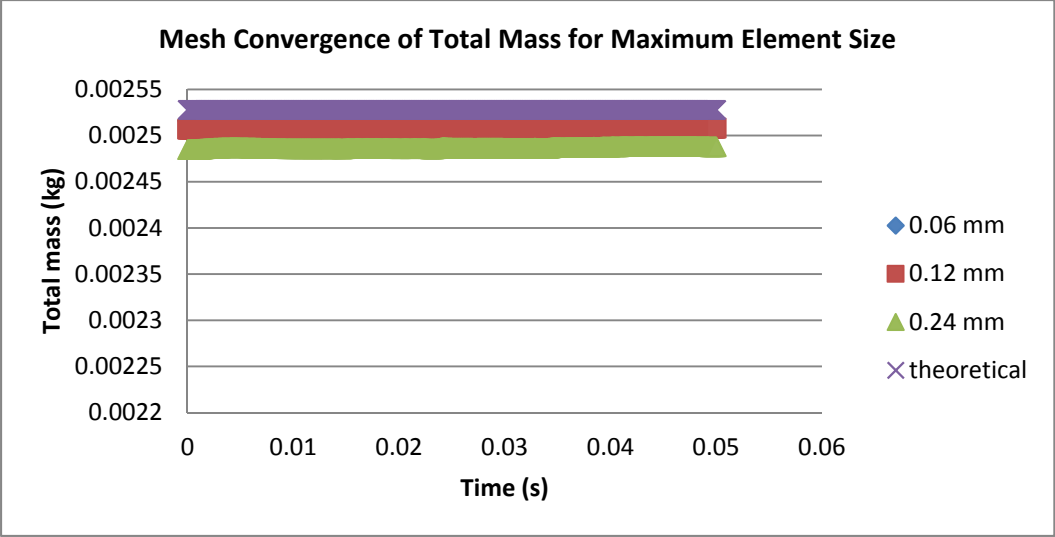


Figure A3. Mesh convergence in 3.0 mm diameter droplet model.

The above mesh convergence shows that as the maximum element size was decreased to 0.06 (blue), the total mass converges to the actual total mass (yellow line), shown by their overlap. This allows for the assumption of successful mesh convergence to be met.

## **Appendix C: References**

- [1]. Colton, Clark K. (2014). Oxygen Supply to Encapsulated Therapeutic Cells. *Advanced Drug Delivery Review*.
- [2] Nicodermus, Garret. (2008). Cell Encapsulation in Biodegradable Hydrogels for Tissue Engineering Applications. *Tissue Engineering*.
- [3]. Ma, Minglin. (2013). Core-Shell Hydrogel Microcapsules for Improved Islets Encapsulation. *Advanced Healthcare Materials*.
- [4]. Luo, Dan. (2013). Enhanced transcription and translation in clay hydrogel and implications for early life evolution. *Scientific Reports*.
- [5]. Park, Hongkwan. (2012). Fabrication of Cross-Linked Alginate Beads Using Electrospraying for Adenovirus Delivery. *International Journal of Pharmaceutics*.